

# Measurement of the Rates of Production and Dissipation of Turbulent Kinetic Energy in an Energetic Tidal Flow: Red Wharf Bay Revisited

TOM P. RIPPETH, JOHN H. SIMPSON, AND EIRWEN WILLIAMS

*School of Ocean Sciences, University of Wales Bangor, Menai Bridge, Anglesey, United Kingdom*

MARK E. INALL

*University of the Highlands and Islands Project, Scottish Association for Marine Science, Dunstaffnage Marine Laboratory, Oban, United Kingdom*

(Manuscript received 6 November 2001, in final form 17 March 2003)

## ABSTRACT

Simultaneous measurements of the rates of turbulent kinetic energy (TKE) dissipation ( $\varepsilon$ ) and production ( $P$ ) have been made over a period of 24 h at a tidally energetic site in the northern Irish Sea in water of 25-m depth. Some  $\varepsilon$  profiles from  $\sim 5$  m below the surface to 15 cm above the seabed were obtained using a fast light yo-yo (FLY) microstructure profiler, while  $P$  profiles were determined from a bottom-mounted high-frequency acoustic Doppler current profiler (ADCP) using the variance method. In homogeneous flow of the kind observed, the turbulence regime should approximate to local equilibrium so that, with no buoyancy forces involved,  $\varepsilon$  and  $P$  are expected to covary with mean values that are equal. The results show a close tracking of  $\varepsilon$  and  $P$  for most of the observational period. For the second tidal cycle, when there was no significant surface wave activity, a mean ratio of  $\varepsilon/P \approx 0.63 \pm 0.17$  was obtained. Although this is a significant deviation from unity, it is within the range of uncertainty previously reported for the  $\varepsilon$  measurements. A marked phase lag of between 5 and 20 min between the maximum  $P$  and the maximum  $\varepsilon$  is interpreted using a simple model in terms of the decay rate of TKE. Consideration of inherent instrument noise has enabled an estimate of the lowest  $P$  threshold measurable using the variance technique. For the chosen averaging parameters a value of  $P_{\min} \sim 7 \times 10^{-5} \text{ W m}^{-3}$  is estimated. Two other significant differences between the two sets of measurements are attributed to errors in the stress estimate. The first is a bias in the estimate of stress resulting from a combination of instrument tilt ( $1^\circ$ – $3.5^\circ$ ) and surface wave activity. The second are anomalously high stress estimates, covering nearly one-half of the water column at times, which are thought to be due to instrument noise associated with the large wave orbital velocities.

## 1. Introduction

In the 1950s and 1960s, Red Wharf Bay, on the east coast of the Island of Anglesey, United Kingdom, was the setting for the important pioneering studies of turbulence and associated shear stresses in tidal flows by K. Bowden and his coworkers at Liverpool University. They investigated the distribution of shearing stresses in a tidal current by integrating the equations of motion upwards from the bottom boundary, using a value of bed stress found either from measurements in the near-bed log layer or from measurements of the sea-surface slope (Bowden et al. 1959). Bowden and Fairbairn (1956) used the then newly available electromagnetic current meter mounted on a tripod that sat on the seabed, to measure all three components of turbulent velocity

fluctuations in a tidal current. Although limited to a few fixed points at heights close to the seabed, these measurements allowed the direct estimation of the Reynolds stresses in the flow, which were combined with measurements of velocity shear to give estimates of the rate of production of turbulent kinetic energy (TKE). We have recently revisited Red Wharf Bay to make simultaneous estimates of the rate of production ( $P$ ) and dissipation ( $\varepsilon$ ) of TKE that extend through most of the water column.

The new measurements depend on two independent observational techniques: for the measurements of production we have exploited recent advances in high-frequency acoustic Doppler current profiler (ADCP) technology which allow the remote estimation of Reynolds stress profiles (Tropea 1981; Lohrmann et al. 1990). This technique, known as the “variance” method, relies on differencing velocity variances along opposing beams and has been employed in a number of shelf and estuarine studies of the evolution of the structure of turbulence (Stacey et al. 1999a,b; Lu and Lueck 1999;

---

*Corresponding author address:* Tom Rippeth, School of Ocean Sciences, University of Wales Bangor, Menai Bridge, Anglesey LL59 5AB, United Kingdom.  
E-mail: t.p.rippeth@bangor.ac.uk

Lu et al. 2000; Rippeth et al. 2002). In broadband instruments operating at high frequency (1.2 MHz), the temporal and spatial resolution permits estimates of both the shear stress and the mean shear, and hence  $P$  on scales down to 25 cm.

For the determination of  $\varepsilon$  we have used the fast light yo-yo (FLY) free-fall probe (Dewey et al. 1987). This type of profiler has been successfully applied in a number of recent observational campaigns designed to improve our understanding of the interaction between turbulence, stratification, and shear in shelf seas (Simpson et al. 1996; Lien and Gregg 2001; Inall et al. 2000; Moum and Nash 2000; Rippeth et al. 2001) and estuaries (Etemad-Shahidi and Imberger 2002; Inall and Rippeth 2002).

Here,  $P$  and  $\varepsilon$  are the leading terms in the TKE equation. For horizontally uniform conditions with a well-mixed water column, the TKE equation simplifies to

$$-\frac{\partial}{\partial z} \left( K_q \frac{\partial E}{\partial z} \right) + \frac{\partial E}{\partial t} = -\tau_x \frac{\partial \bar{u}}{\partial z} - \tau_y \frac{\partial \bar{v}}{\partial z} - \varepsilon = P - \varepsilon, \quad (1)$$

where  $K_q$  is a diffusion coefficient and

$$E = \frac{q^2}{2} = \frac{1}{2}(u'^2 + v'^2 + w'^2). \quad (2)$$

In tidally energetic flows the time derivatives and diffusion terms are usually small in relation to  $P$  and  $\varepsilon$  and, under the assumption of local equilibrium, may be neglected so that, as a first approximation, we expect  $P \approx \varepsilon$ .

In this paper we present and compare what we believe to be the first series of simultaneous and independent measurements of  $P$  and  $\varepsilon$  covering a large proportion of the water column, at a site with a strong tidal flow where the water column can be considered to be well mixed. It is widely recognized that production and dissipation will balance and so the experiment provides a critical comparison of the two profile methods employed. We shall identify significant differences between the two sets of measurements, in terms of their accuracy and noise levels, and offer an interpretation of the phase relation between  $P$  and  $\varepsilon$  in terms of the decay rate of TKE.

## 2. Location and observational methods

### a. Red Wharf Bay

The new observations for the comparison were undertaken at a site (53°22.8'N, 4°12.5'W) close to the site of Bowden's original observations in Red Wharf Bay, approximately 4 km from the east coast of Anglesey (Fig. 1). The water depth at the site varied between ~23 m at low water and ~28 m at high water; the seabed was composed mostly of muddy sand. The tidal currents at this site are almost rectilinear (i.e., the

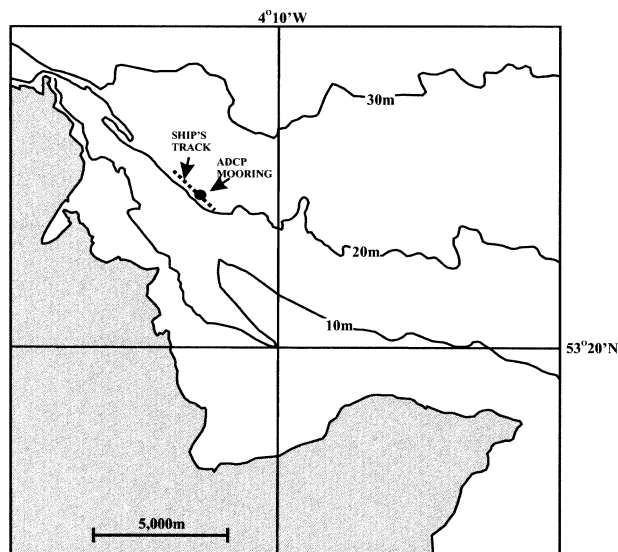


FIG. 1. Map of the Red Wharf Bay area showing the position of the observations, the topography (the 10-, 20-, and 30-m contours show the depth below chart datum) and the ships' path relative to the ADCP mooring position while the FLY measurements were made (which was always into the tide).

ratio of the minor to major ellipse axes is  $<0.1$ ) and run parallel to the coastline (321°T). During the period of the observations [7–8 July 1998; yeardays (YD) 188–189] the ebb maximum flow was  $\sim 0.65 \text{ m s}^{-1}$  to the northwest with a maximum flood to the southeast of  $\sim 0.85 \text{ m s}^{-1}$ .

During the initial part of the experimental period (up until YD 188.6), shipborne measurements recorded a wind of  $\sim 9\text{--}10 \text{ m s}^{-1}$  blowing from the northwest ( $\sim 320^\circ\text{T}$ ), directly against the ebbing tide. The sea state was moderate and there was a heavy swell. Unfortunately no independent wave measurements are available from this part of the Irish Sea for the time of the observations. The ADCP data reported here have, however, been used to estimate the period of swell to be 5.5 s and wavelength between 60 and 85 m (Howarth 1999). During the afternoon and evening of YD 188 the wind speed diminished to  $3\text{--}5 \text{ m s}^{-1}$  and backed to the southwest, and so the position of the experiment now lay in the wind wake of the Island of Anglesey, thus reducing the fetch, and as a result the sea state dropped to slight by early evening (188.73). These conditions persisted until the following morning (189.31) when the wind, which was now blowing from the west, rose to  $7\text{--}9 \text{ m s}^{-1}$  by midmorning (189.42), leading to a moderate sea state, without significant swell, which persisted to the end of the experiment.

For most of the experiment the water column remained well mixed (i.e., surface to bottom temperature difference  $\Delta T < 0.05^\circ\text{C}$ ) with a water temperature of  $13.5^\circ\text{C}$  and salinity of 35.1. There was some weak stratification in the upper part of the water column around

low water with  $\Delta T_{\max} \sim 0.7^\circ\text{C}$ . This phenomenon occurred during the three low waters sampled and is thought to be the result of the differential advection of a temperature gradient by the sheared tidal flow.

*b. Observational setup*

An internally recording RD Instruments, Inc. (RDI), 1.2-MHz Workhorse ADCP was deployed on the seabed for a period of 25.5 h between 1329 UTC 7 July (approximately 2 h before the local low water) and 1503 UTC 8 July 1998 (YD 188.6–189.6). The ADCP was set up to record the along-beam velocities with a ping rate of 2 Hz. The bin size was set to 1 m and the data were ensemble averaged over 2 s (i.e., four pings). The ADCP was operated in the standard RDI “mode 1.” With the ambiguity velocity set to  $1.7 \text{ m s}^{-1}$ , the standard deviation of the uncertainty associated with each along beam velocity estimate is  $\pm 0.007 \text{ m s}^{-1}$  (RDIplan Software). The instrument was mounted on a heavy purpose built frame and sat approximately flat on the sea bed with a heading of  $321^\circ\text{T}$ ; that is, beams 3 and 4 were aligned with the axis of the tidal flow. In situ pitch and roll measurements indicated that initially the instrument was inclined ( $\psi_{34}$ ) at approximately  $\psi_{34} \sim -3.5^\circ$ , but that the frame settled slowly as the deployment progressed with  $\psi_{34} < 2^\circ$  within 8 h finally settling to  $\sim 1^\circ$  after 14 h. The roll ( $\psi_{12}$ ) was less significant, with  $\psi_{12} \sim 0.5^\circ$  at the beginning of the deployment gradually shifting to  $-0.2^\circ$  by the end of the deployment. RDI (1998) quote the precision of the pitch-and-roll gauges to be  $0.1^\circ$ .

The FLY profiler falls freely at a speed of  $0.7\text{--}0.8 \text{ m s}^{-1}$  and measures components of the horizontal velocity via a piezoelectric sensor, which detects the force exerted on two small aerofoil probes by the transverse flow. This force, which is proportional to the along-stream horizontal velocity, is differentiated to give the velocity shear on scales down to  $\sim 1.5 \text{ cm}$ . Estimates of the rate of dissipation per unit volume,  $\varepsilon$ , are derived from the mean-square shear from each probe using a relationship for isotropic turbulence:

$$\varepsilon = 7.5\mu \int_{k_l=0}^{k_u=\infty} k_3^2 \varphi_{11}(k_3) dk_3 = 7.5\mu \left( \frac{\partial u}{\partial z} \right)^2, \quad (3)$$

where  $k_3$  is the vertical wavenumber,  $\varphi_{11}(k_3)$  is the one-dimensional spectrum of the along-stream velocity,  $\mu$  is the dynamic viscosity of seawater, and  $\varepsilon$  is given in watts per cubic meter. The profiler is equipped with a guard ring that allows measurements to be made to within 15 cm of the sea bed. The measurements thus cover almost the entire water column except for a near-surface region ( $\sim 5 \text{ m}$  thick) in which the instrument is accelerating and turbulence may be a result of the ship’s wake.

The FLY profiler was operated from the RV *Prince Madog*, which stayed within  $\sim 500 \text{ m}$  of the mooring

site. A series of 8–16 profiles were made with the FLY every hour between 1445 UTC 7 July and 1432 UTC 8 July 1998. Each series of profiles took between 20 and 30 min to complete, after which the ship returned to the mooring position and a CTD profile was taken.

**3. Data analysis**

*a. High-frequency ADCP*

The along-beam velocities ( $b_i$ , where  $i = 1, 4$ ) were separated into a mean over 10 min  $\bar{b}_i$ , and fluctuating quantity,  $b'_i$ , as

$$b_i = \bar{b}_i + b'_i.$$

The Reynolds stress estimates are calculated using the variance technique proposed by Lohrmann et al. (1990) and described in detail by Stacey et al. (1999a), in which the ADCP is assumed to sit flat on the seabed:

$$\begin{aligned} \frac{\tau_x}{\rho} &= \overline{u'w'} = \frac{\bar{b}_1'^2 - \bar{b}_2'^2}{2 \sin 2\theta}, \\ \frac{\tau_y}{\rho} &= \overline{v'w'} = \frac{\bar{b}_3'^2 - \bar{b}_4'^2}{2 \sin 2\theta}, \end{aligned} \quad (4)$$

where  $\theta$  is the angle each beam makes with the vertical ( $20^\circ$  for the instrument used). The instrument was positioned so that the opposing beams 3 and 4 lay in an approximately coast parallel plane (defined as the  $y\text{--}z$  plane), which was also the principal axis of the tidal flow, and beams 1 and 2 lie in an approximately coastline normal ( $x\text{--}z$ ) plane. Because the surface level varies widely over the tidal cycle we will use height above bed as the vertical coordinate system. ADCP data, which have been collected from bins centered within 1.5 m of the sea surface, are not used because of possible contamination by sidelobe effects.

The estimation of turbulent parameters requires that the velocity field can be assumed to be horizontally homogeneous so that the statistics of the turbulence are the same for each of the four beams (Lu and Lueck 1999). An assumption of stationarity is also necessary and this imposes constraints on the length of record we can use in the analysis. The averaging period must be of sufficient length to provide a good sample of the largest turbulent eddies, but not so long that the turbulent processes cannot be regarded as quasi stationary. In the present case, because our time series are dominated by variability at the semidiurnal frequency, a reasonable compromise between statistical reliability and stationarity is a sample length of 10 min.

The ADCP sampling rate is also a compromise, in this case between temporal resolution and record duration, and involves the averaging of four pings at 0.5-s intervals to give estimates of the along-beam velocity. If the autocorrelation timescale of the velocities does not greatly exceed 2 s, we would expect the variance to be underestimated and with it the Reynolds stress. In

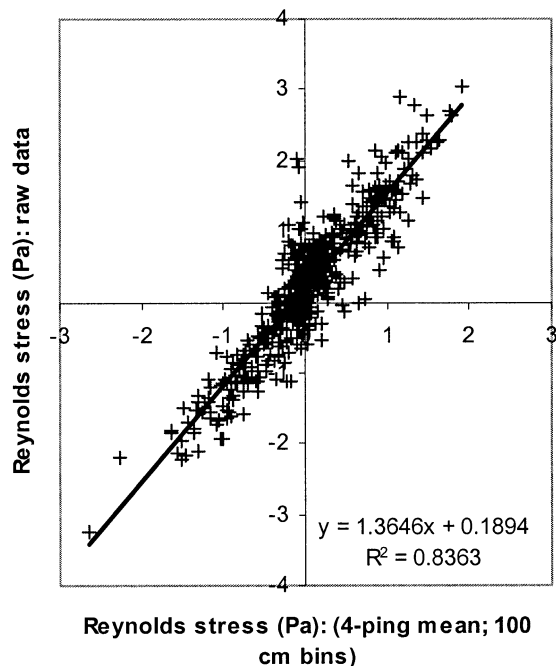


FIG. 2. A comparison of the along-stream Reynolds stress (Pa) calculated using single-ping data from 25-cm bins and from four-ping average data from 1-m bins for a single tidal cycle deployment in Menai Strait [see Rippeth et al. (2002) for details]. The fit has an  $r^2 = 0.84$  with 1080 degrees of freedom and gives a gradient of 1.36.

addition there may be some apparent loss of stress due to the bin size being comparable in scale to some of the smaller eddies that are involved in momentum transfer in the vertical. We have used the data from the single tidal cycle deployment of the ADCP (in mode 1) in a tidal channel to investigate these effects on stress estimates (Rippeth et al. 2002). Figure 2 shows a comparison of the along-channel stress estimated from single ping data using 25-cm bins with that estimated from four-ping mean data with 1-m bins. Regression analysis of  $\sim 12$  h of data collected in the Menai Strait (Rippeth et al. 2002) indicates that the stresses estimated from the 1-m-bin four-ping averages are underestimated by  $\sim 27\%$  relative to the single-ping 25-cm bin-size results. We have therefore applied a correction of 1.36 to all of our stress estimates.

The rate at which energy is transferred from the mean flow to turbulent kinetic energy through the interaction of the turbulence with the shear is estimated from the product of the Reynolds stress and the velocity shear according to

$$P = -\tau_x \frac{\partial \bar{u}}{\partial z} - \tau_y \frac{\partial \bar{v}}{\partial z} = -\rho \left( \overline{u'w'} \frac{\partial \bar{u}}{\partial z} + \overline{v'w'} \frac{\partial \bar{v}}{\partial z} \right), \quad (5)$$

where both the stress and velocity shear are estimated from the ADCP data. As a result of the alignment of the ADCP to the tidal flow, we would expect the main contribution to the rate of production to come from the second term on the right-hand side of Eq. (5).

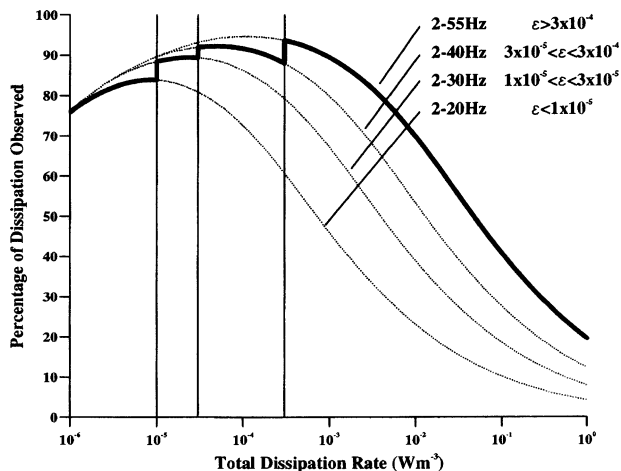


FIG. 3. An estimate of the percentage of the actual dissipation rate measured by imposing finite integration limits. This plot is for a typical molecular viscosity and instrument fall speed. The estimates are based on the Nasmyth (1970) form of the Kolmogorov spectrum.

#### b. $\epsilon$ profiler

The mean-square shear is calculated from the FLY data by first deriving the power spectrum for each section of the record [depth interval  $\sim 1$  m, although this is reduced near the bed to maintain homogeneity following the method of Dewey et al. (1987)]. This allows the application of the Ninnis spectral correction for the roll-off of the shear probe response at high frequencies due to the effects of spacial averaging (Ninnis 1984), and the elimination of high-frequency noise through application of finite integration limits in evaluating (3). A correction is then applied to boost the estimate of  $\epsilon$  to account for the use of the finite integration limits. The correction is estimated by matching the total energy observed between the high- and the low-frequency cut-off points to a form of the Kolmogorov spectrum derived empirically by Nasmyth (1970). The upper-frequency limit for the direct estimate of  $\varphi_{11}(k_3)$  is normally set to 55 Hz, at which point the shear probe response is reduced by a factor of 50%. For a typical fall speed of  $w = 0.7$  m s $^{-1}$  this gives a half-power wavenumber of  $k_u = 79$  cpm. In order to minimize noise contamination, this limit is further reduced for estimates of  $\epsilon < 3 \times 10^{-4}$  obtained from the initial integration. A high-frequency cutoff of 40 Hz is applied for initial  $\epsilon$  estimates in the range  $3 \times 10^{-5} < \epsilon < 3 \times 10^{-4}$ , of 30 Hz for  $10^{-5} < \epsilon < 3 \times 10^{-5}$ , and of 15 Hz for  $\epsilon < 10^{-5}$  W m $^{-3}$ . A low-frequency limit is set at 2 Hz, corresponding to  $k_1 = 2.4$  cpm for a fall speed of  $0.7$  cm s $^{-1}$ , to prevent any energy leakage from the mean flow. The value of  $\epsilon$  obtained from the integration is then boosted to account for the imposition of finite integration limits. The factor by which  $\epsilon$  is boosted is applied to the two shear probes independently and generally represents a small percentage of  $\epsilon$ , only exceeding 20% at high dissipations ( $> 10^{-2}$  W m $^{-3}$ ) as shown in Fig. 3.

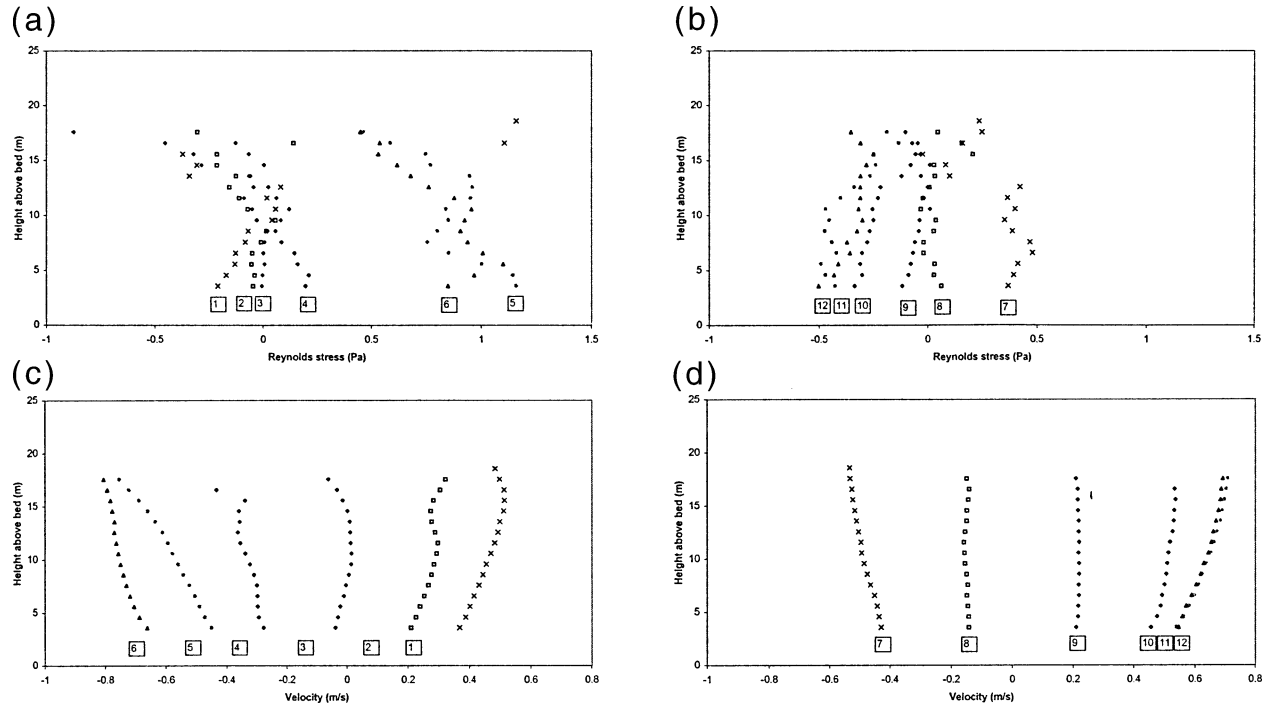


FIG. 4. (a),(b) Hourly mean Reynolds stress (Pa) profiles for the first 12 h of the experiment. The boxed numbers indicate the time of the profile in yeardays. (c),(d) Mean velocity ( $\text{m s}^{-1}$ ) profiles at times corresponding to the stress profiles in (a).

Uncertainties in the measurements of  $\epsilon$  have been described in detail (e.g., Oakey 1982; Lueck et al. 1983; Dewey and Crawford 1988; Moum et al. 1995) and so will only be briefly presented here. There are a number of unavoidable factors that can contribute to a potential uncertainty in each  $\epsilon$  estimate of  $\sim \pm 50\%$ . These consist of random errors and systematic offsets. The main sources of random errors are 1) uncertainties in flow rate variations past the shear probes, which are generally assumed to equal the fall speed of the instrument ( $\epsilon \propto w^4$ ) and contribute to an uncertainty of  $\sim 20\%$  to the final value of  $\epsilon$  (Dewey and Crawford 1988); 2) systematic bias in the estimation of  $\epsilon$  that arise because of uncertainties in the shear probe calibration (7%), deviations in the electronic transfer function (2%), and uncertainty in the estimate of dynamic viscosity,  $\mu$  (5%) (Dewey and Crawford 1988). Other potential biases in the estimation of  $\epsilon$  are associated with the use of the Ninnis function to correct for shear probe roll off and the Nasmyth spectrum to correct for the finite integration limits used in (3) (Oakey 1982; Moum et al. 1995; Gregg 1999) and the sensitivity of the shear probe calibration to temperature (Osborne and Crawford 1980).

Comparison of the estimated values of  $\epsilon$  for each of the two shear probes shows a mean ratio of  $\epsilon_1/\epsilon_2 = 1.073 \pm 0.026$ . The ratio increases only very slightly during the 24 h of measurements (for the last 8 h of data a mean ratio of  $1.113 \pm 0.025$  was obtained), showing a small drift in the relative calibrations of the two

probes. The close agreement between the two shear probes gives confidence that both shear probes behaved well throughout the measurement period.

#### 4. Results

##### a. The current and Reynolds stress profiles

The 1-h mean vertical stress profiles acting in the direction parallel to the direction of the tidal flow are given (Figs. 4a,b) together with the corresponding along-stream current profiles (Figs. 4c,d) for the full period of the observations. The velocity profiles show maximum near surface flood flows of  $>0.8 \text{ m s}^{-1}$ . (e.g., profiles 5 and 6) while the maximum near-surface ebb flows are  $\sim 0.6 \text{ m s}^{-1}$ . (e.g., profiles 1, 10, 11, 12). The largest velocities are generally observed near the surface with the velocities in the lower part of the water column conforming to a logarithmic profile.

The stresses generally (e.g., profiles 10 and 12) decrease linearly with height above the bed from an extreme (up to  $\sim 1 \text{ Pa}$ ) near the seabed (height = 3.5 meters above the seabed) to negligible values near the surface. Around both of the high waters (e.g., profiles 8 and 9) there is negligible stress throughout the water column. There are, however, exceptions with profiles that show high stress ( $0.5\text{--}1 \text{ Pa}$ ) in the upper part of the water column (e.g., profiles 1, 2, and 3). These occur during the latter part of the first and second ebb flows

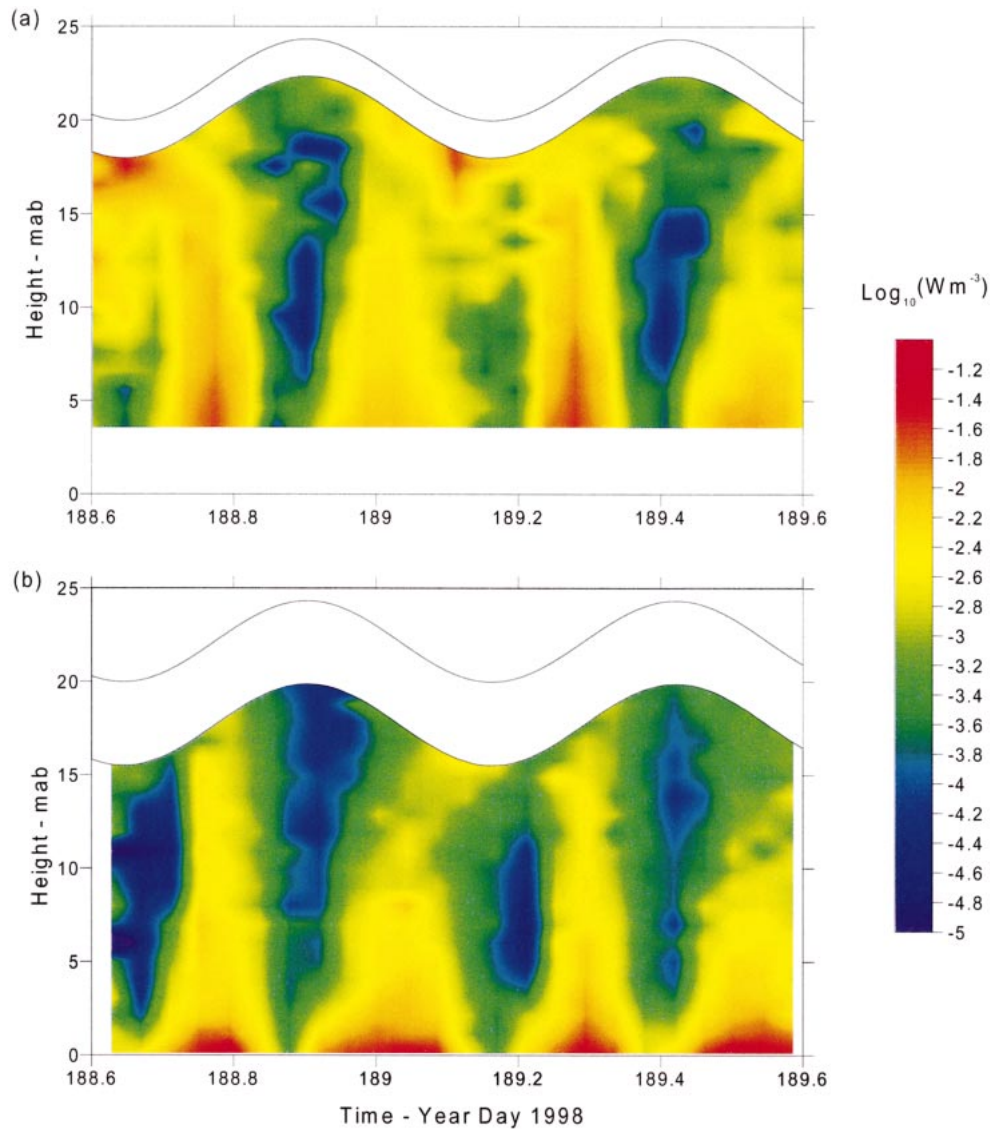


FIG. 5. Contour plots of the rate of (a) production and (b) dissipation of TKE ( $\log_{10} \text{W m}^{-3}$ ). The data have been interpolated onto a 1 h by 1 m grid prior to contouring.

and both of the low waters sampled. There are also profiles that show a linear decrease in stress from values of  $\sim 0.5$  Pa to near zero in the middle of the water column, extending to the surface. A further interesting observation is the “curling back” of the stress profile in the bottom two bins during maximum flow (e.g., profile 12), with a maximum stress of  $\sim 1.1$  Pa observed at a height of 3.5 m above the seabed decreasing to  $\sim 0.8$ – $1.0$  Pa at a height of 1.5 m above the seabed (mab).

*b. Estimates of the rate of production and dissipation of turbulent kinetic energy*

Contour plots of the time series of the rates of production and dissipation of turbulent kinetic energy are

given in Fig. 5 and show many common features between the two time series. There is a one-quarter diurnal variation in both  $P$  and  $\epsilon$  which is clearly related to the phase of the tidal current. The largest values of both parameters ( $\sim 3 \times 10^{-2} \text{W m}^{-3}$ ) are observed near the seabed around maximum flood, falling off ( $\sim 5 \times 10^{-5} \text{W m}^{-3}$ ) around slack water, and increasing to a second maximum at maximum ebb ( $\sim 10^{-2} \text{W m}^{-3}$ ). Both parameters decrease with height above the seabed, with a reduction of about 1.5 orders of magnitude at 15 mab. The major difference between  $P$  and  $\epsilon$  is that there are high values of  $P$  near to the surface and these are strongest ( $\sim 10^{-2} \text{W m}^{-3}$ ) during the latter part of the first ebb and the first low water. Similarly enhanced values of  $P$  are evident during the second ebb and low water

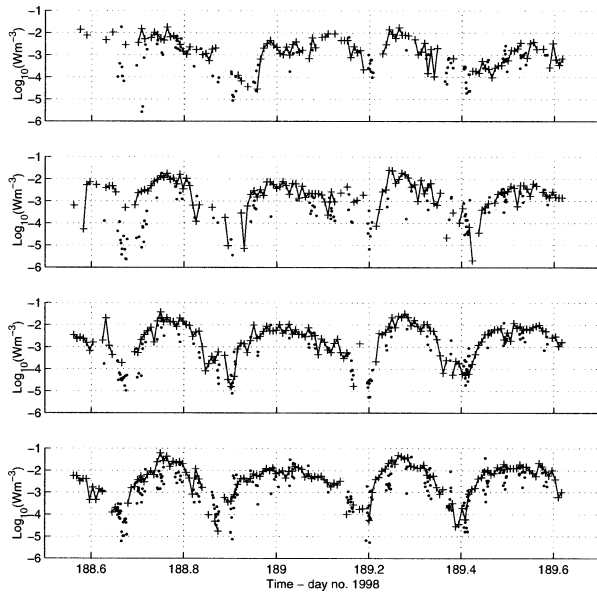


FIG. 6. Time series of the rate of production (crosses) and dissipation (solid dots) of TKE at heights of (a) 15.5, (b) 10.5, (c) 6.5, and (d) 3.5 m above the seabed. Breaks in the time series of  $P$  are indicative of negative values of  $P$ .

although the difference between the two parameters is not so great as during the first tidal cycle.

Time series for four different levels through the water column are shown in Fig. 6. This method of presentation again shows how well the two parameters track each other. Also included in this plot is the frequency of negative  $P$  estimates. In appendix A, we demonstrate that these negative values are a result of a lack of coherence between the stress and shear estimates due to the influence of noise, and they provide a measure of the quality of the data. By comparing the distribution of  $\epsilon$  with the distribution of the negative  $P$  values around the two low waters sampled we have estimated the low cutoff for the measurement of  $P$ , using this technique and the chosen parameter settings, is  $\sim 7 \times 10^{-5} \text{ W m}^{-3}$ . The large number of negative values observed near the surface early in the observations, together with the large estimates for near surface stress are shown to fail the “significance of covariance test” (appendix A). This result leads us to conclude that the observed discrepancies between the  $P$  and  $\epsilon$  estimates in the upper part of the water column are a result of corruption of the stress estimates by noise, which is thought to be associated with the large wave orbital velocities resulting from the strong surface wave activity at those times.

*c. Comparison of  $P$  and  $\epsilon$*

The ratio of the rates of dissipation to production of turbulent kinetic energy has been calculated for the first and second tidal cycles separately, following the removal of  $P$  estimates made during periods when the

TABLE 1. The ratio of  $\epsilon/P$  estimated for the main dataset together with estimates for subsamples of the dataset covering the first and second flood tides and the first and second ebb tides. The 95% confidence limits of the ratios have been calculated using a bootstrap resampling technique.

Data subset	$\epsilon/P$	$\epsilon_+/P_-$	$\epsilon_-/P_+$
All data	0.523	0.456	0.626
Tidal cycle 1	0.479	0.393	0.582
Tidal cycle 2	0.629	0.489	0.807
Flood 1	0.309	0.242	0.396
Flood 2	0.658	0.435	0.981
Ebb 1	0.853	0.687	1.058
Ebb 2	0.607	0.479	0.766

stress estimates are unreliable (i.e., around slack water, near the surface early on). The quantitative comparison between  $P$  and  $\epsilon$  was made by calculating the individual ratios of  $P$  with the corresponding values of  $\epsilon$ . The ratios for each of the two tidal cycles together with those for the flood and ebb sections of each tidal cycle are shown in Table 1.

The ratio for the second tidal cycle of measurements, when surface wave activity was weak, is  $0.629 \pm 0.15$ . The error shown is the 95% confidence limits of the ratios calculated using a bootstrap resampling technique. During this tidal cycle the ratios of  $\epsilon/P$  on the flood and ebb, 0.658, and 0.607, are not significantly different from one another. The ratio of  $\epsilon/P = 0.629 \pm 0.15$  for the second tidal cycle is the main result of the paper. It is a significant deviation from the expected value of unity. It implies that either the dissipation rate measured using the profiler is underestimated, or that the production rate estimated using the ADCP variance method is too large. A full discussion of this result will be given in section 5.

The ratio of  $\epsilon/P$  for the first tidal cycle is  $0.479 \pm 0.09$ . In contrast to the second tidal cycle, the ratios for the two phases of the first tidal cycle of observations, at which time there was significant surface wave activity particularly when the wind blowing directly against the ebbing tide, are very different. A flood ratio of 0.309 was obtained which may be compared with an ebb ratio of 0.853. The stability of the two independent estimates of  $\epsilon$  implies that the likely error causing the difference in the ratio is a bias in the estimate of  $P$ . Because the ratio is invariant with depth a bias in the estimate of stress would appear the likely cause.

In order to check for bias in the along-stream stress, two estimates of the friction velocity are made:  $U_{*s}$  = the stress estimate for the first ADCP bin (centered at 3.5 mab) via the variance method, and  $U_{*p}$  which is determined from the mean along-stream velocity profile via a logarithmic fit (following Lueck and Lu 1997). By assuming that the profile estimate is not influenced, to first order, by instrument tilt or surface waves, we use  $U_{*p}$  to normalize the stress estimate in the bottom ADCP bin. A regression analysis shows that during the

ebb phase of the tide a ratio of  $U_{*S}/U_{*P} \sim 0.69$  is obtained which may be compared with the flood value of  $U_{*S}/U_{*P} \sim 1.25$ . Dividing the data into the two tidal cycles gives ratios of 0.56 and 0.90 during the first and second ebb tides, respectively, and 1.43 and 1.0 during the first and second flood tides, respectively. These results show the values obtained for the second tidal cycle are not significantly different from one another, nor from the expected value of unity. However, there is a significant departure in  $U_{*S}/U_{*P}$  from the expected value of unity during the first tidal cycle.

The variation in the ratio  $U_{*S}/U_{*P}$  implies that there is an  $\sim 50\%$  bias in the stress during the first tidal cycle. This bias results in an overestimate of the stress on the flood phase of the tide and an underestimate on the ebb. As a consequence  $P$  will be overestimated on the flood and underestimated on the ebb. The magnitude of the resultant bias in  $P$  is consistent with the observed flood/ebb variation in the ratio  $\varepsilon/P$  for the first tidal cycle.

The main difference in conditions between the two tidal cycles sampled was that during the first cycle, there was strong but declining surface wave activity, which had died away by the time we began the second tidal cycle of observations. In appendix B we present a simple linear wave model with which we are able to estimate the magnitude of the bias in the stress resulting from the combination of the tilt of the ADCP and the presence of surface waves. The predicted bias is consistent with the bias implied from the ratio of the friction velocities ( $U_{*S}/U_{*P}$ ). We therefore strongly suggest that the variations in the ratio of  $\varepsilon/P$  between the first and second tidal cycles sampled, and the flood and ebb of the first tidal cycle, are a result of a bias in the stress estimates made during the first tidal cycle using the variance method, which is a consequence of a combination of surface wave activity and ADCP tilt.

#### d. $M_4$ analysis

To further examine the time dependence of the rate of production and dissipation of TKE in the lower part of the water column, the data were fitted to a one-quarter diurnal constituent ( $M_4$ ) of the form (e.g., Simpson et al. 1996):

$$X = a_0 + a_4 \sin(\omega_4 t - \varphi_4), \quad (6)$$

where  $a_0$  represents the mean  $P$  or  $\varepsilon$  over the tidal cycle and  $a_4$  and  $\varphi_4$  are the amplitude and the phase lag of the temporal variations in the signal at a frequency corresponding to the  $M_4$  tidal constituent. A least squares procedure is used to fit Eq. (6) to the production and dissipation time series at each level in the water column.

The results (Fig. 7) show a decrease in the mean rate,  $a_0$ , and quarter-diurnal amplitude,  $a_4$ , of production and dissipation with height above the bed, with generally higher values for the production. The mean value of  $\varepsilon$  is approximately one-half of the mean value of  $P$ . The amplitude of the one-quarter diurnal variation in  $\varepsilon$  is

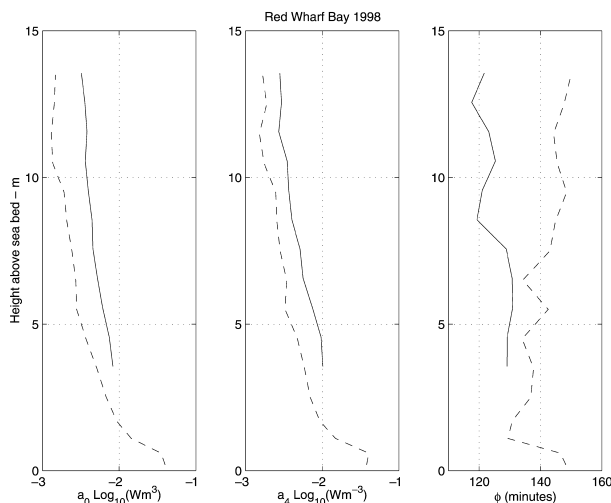


FIG. 7. Resultant profiles of a least squares fit of a quarter-diurnal signal to the production (solid line) and dissipation (broken line) measurements: (a) the mean value  $a_0$ , (b) the amplitude of the variation  $a_4$ , and (c) the phase lag of the variation  $\varphi$ .

$\sim 65\%$  of the amplitude of  $P$ . There is a significant lag in the timing of maximum  $\varepsilon$  after maximum  $P$  of 5–10 min near the bottom of the water column, which increases to  $\sim 25$  min above  $\sim 8$  mab.

We can understand this phase lag in terms of a simple analytical model. For a homogeneous fluid and neglecting diffusion of TKE [Eq. (1)] reduces to

$$\frac{\partial E}{\partial t} = P - \varepsilon. \quad (7)$$

We take the production term  $P$  from the model of an oscillating boundary layer at frequency  $\omega$  with uniform  $N_z$  (Simpson et al. 2000; after Lamb 1932), which gives

$$\begin{aligned} P &= N_z \left( \frac{\partial u}{\partial z} \right)^2 \\ &= N_z \left( \frac{A\beta}{\omega} \right)^2 e^{-2\beta z} \left[ 1 + \cos \left( 2\omega t - 2\beta z - \frac{\pi}{2} \right) \right], \end{aligned}$$

where  $z$  is the height above the bed,  $\beta = \sqrt{(\omega/N_z)}$ ,  $\omega$  = the M2 tidal frequency and  $A$  is the amplitude of the forcing by the tidal pressure gradient. At each level  $P$  can therefore be written as

$$P = B(z) \{ 1 + \cos[2\omega t - \varphi(z)] \},$$

substituting into (12) and setting  $\varepsilon = \alpha E$  where the proportionality  $\alpha$  may be a function of  $z$ , and  $1/\alpha$  is the decay rate for turbulent kinetic energy.

We readily find a solution of  $E$  as

$$E(z, t) = \frac{B(z)}{\alpha} + \frac{B(z)}{\sqrt{\alpha^2 + 4\omega^2}} \cos(2\omega t - \gamma), \quad (8)$$

where  $\gamma = \tan^{-1} 2\omega/\alpha$ . From the observed value of the

phase difference ( $\gamma \sim 25^\circ$  at 10 mab), we can estimate  $1/\alpha$ , which is the  $1/e$  decay time of the TKE as  $\sim 2000$  s.

This may be compared with the decay rate estimated from, for example, the Mellor–Yamada closure with an algebraic length scale  $L$ , which gives  $\varepsilon$  as

$$\varepsilon = \frac{(2E)^{3/2}}{B_0 L}, \quad (9)$$

where the length scale  $L = \kappa_0 z(1 - z/H)^{1/2}$ , and  $H$  is the water depth and  $B_0$  a constant  $\sim 15$ . The corresponding decay time from an initial level of  $E = 3 \times 10^{-3} \text{ W m}^{-3}$  at  $z = 10$  mab, where  $L = 2$  m, would be  $\sim 4200$  s. This is about 2 times the value we obtain from our observations.

## 5. Summary and discussion

The bottom-mounted ADCP measurements in parallel with frequent profiles using a microstructure probe have provided simultaneous 25-h time series of flow, structure, and turbulence parameters at a site with a rectilinear tidal current of amplitude  $\sim 0.8 \text{ m s}^{-1}$ . The water column remained well mixed for much of the observational period and strong surface wave activity at the start of the experiment diminished to low levels as the experiment progressed. The results are useful in two ways. First, they provide a set of observations that define the cycles of the production and dissipation of TKE in a well-mixed shelf seawater column. Second, they allow us to test the two techniques employed, since we would expect  $\varepsilon$  and  $P$  to closely track each other and covary with mean values that are equal. There is good agreement between the patterns of variation of  $P$  and  $\varepsilon$ . Both parameters closely track each other and follow a quarter-diurnal pattern although there is a phase delay in dissipation relative to production of between 5 and 25 min. We have used this phase difference to estimate  $\alpha$ , which is a measure of the rate of decay of TKE, and the values obtained are shown to be about one-half of those obtained from the Mellor and Yamada turbulence closure scheme.

The main discrepancy between the  $P$  and  $\varepsilon$  estimates made in near-ideal conditions (i.e., the second tidal cycle of measurements) is that the ratio of  $\langle \varepsilon/P \rangle$  is not the expected value of unity, but  $= 0.63 \pm 0.17$ , a value that does not vary significantly with height above the seabed within the domain of the overlapping measurements. This discrepancy is considerably less than those reported for other comparisons of in situ measurements of marine turbulence. For example, Lu et al. (2000) found  $\varepsilon/P \sim 0.2$  for midwater column estimates of  $P$  using the variance method and  $\varepsilon$  measured at one height using a moored velocity shear probe. A rigorous comparison of the precision of midrange values of  $\varepsilon$  measured in an oceanic location using two free-fall velocity shear probes simultaneously gave a difference of a factor of 2 (Moum et al. 1995).

There are a number of uncertainties in the calculation of  $\varepsilon$  that may result in a bias.

- 1) Dewey and Crawford (1988) estimate a potential bias of up to 14% arising out of uncertainties in the calibrations applied in conversion of voltage to velocity shear.
- 2) A further bias may arise out of the neglect of the effect of temperature on the shear probe sensitivity. Here the temperature difference between the water column in Red Wharf Bay and the water bath in which the calibrations were undertaken was  $\sim -6.5^\circ\text{C}$ , which could lead to an underestimate in  $\varepsilon$  of  $\sim 12\%$ – $25\%$  (R. G. Lueck 2001, personal communication).

A number of more fundamental concerns have been raised about this method, in particular relating to the following.

- 1) The Ninnis response function used to account high wavenumber sensor rolloff. Discrepancies between the Ninnis spatial response function and a second estimate of the spatial response function by Oakey (1982) suggests doubts over the accuracy of observations in regions of very high dissipations (Gregg 1999). The spacial response function of the type of aerofoil probe used here is currently being investigated and could potentially offer an explanation for the discrepancy between the  $P$  and  $\varepsilon$  estimates reported here (Macoun and Lueck 2003, manuscript submitted to *J. Atmos. Oceanic Technol.*).
- 2) The use of the Nasmyth spectrum to correct for the spectral loss of variance resulting from the application of finite integration limits (Moun et al. 1995; Gregg 1999). To minimize any error we have only used this spectrum to add extra variance, and so any bias will be restricted to the higher values of  $\varepsilon$  and will be small in comparison with the other bias identified.

By examining sections of the data, we have shown that during the first of the tidal cycles sampled there is a significant bias in the  $P$  estimate, which is sensitive to the direction of the tidal flow, resulting in a considerably smaller ratio on the flood than on the ebb. Because this bias is not present in the ratios calculated for the second tidal cycle we conclude that it is a result of the significant surface wave activity experienced in the early part of the observational period. We have shown, through estimates of the friction velocity based on fits of the observed velocity profiles to a logarithmic profile, which we assume to be insensitive to surface wave activity, and using the along-stream stress estimate from the lowest ADCP bin, that the bias in the  $P$  estimates during the first tidal cycle may be explained by a bias in the stress estimate. Using a linear wave model we have shown that this bias in the stress may be explained as a consequence of the tilt in the ADCP and surface wave activity.

We have thus identified the following features associated with the ADCP variance method:

- corruption of the stress estimate by noise, resulting from surface wave activity;
- a bias in the stress estimate due to a combination of instrument tilt and surface wave activity [it should be noted that the bias is significant even at small ( $\sim 2^\circ$ ) tilts]; and
- a low threshold for the estimate for the rate of production of TKE of  $\sim 7 \times 10^{-5} \text{ W m}^{-3}$  (for the instrument setup used here), which is significantly larger than the theoretical estimate [it should be noted that this figure may be significantly improved upon by using the new RDI mode-12 multiplying option (Williams and Simpson 2003, manuscript submitted to *J. Atmos. Oceanic Technol.*)].

*Acknowledgments.* Ray Wilton (UWB) and Alan Harrison (Proudman Oceanographic Laboratory) provided invaluable technical support. Our thanks go also to Captain Steve Duckworth and the officers and crew of the RV *Prince Madog* for their assistance in making the measurements reported here. Tom Rippeth is in receipt of a NERC research fellowship and Eirwen Williams is in receipt of a NERC studentship. The data collection was supported by the EU MAST III PROVESS project (Contract MAS3-CT97-0159) and data analysis was completed with support from the EU Framework V Mabene project (Contract EVK3CT-2002-000761).

## APPENDIX A

### Negative Stress Estimates and the Low Production Threshold

Negative estimates of  $P$  are obtained (Fig. 5) typically around slack water, and in the upper part of the water column around low water. Lu and Lueck (1999) similarly report negative  $P$  estimates, using this technique, at times of weak flow. These indicate either a lack of coherence between the stress and shear estimates due to the influence of noise, or the transfer of energy from turbulence into the mean flow. In order to test for the former, a “significance of covariance” test given by Lueck and Wolk (1999) is applied. The method involves decomposing the covariance terms in Eq. (4) into two time series with zero lag; that is,

$$\overline{b_2'^2} - \overline{b_1'^2} = \overline{(b_2' + b_1')(b_2' - b_1')}. \quad (\text{A1})$$

If one time series is shifted by phase lag or lead which is significantly larger than the decorrelation timescale ( $\leq 15$  s), the statistical nature of the time series will remain unchanged, but it will have no correlation with the other time series, on average. A distribution of this random covariance is then obtained by choosing many different (300) lag times and then computing the covariance. If the zero lag covariance (i.e., the stress es-

TABLE A1. Estimates of Reynolds stress in the direction of the tidal flow together with the 95% significance level ( $\Delta_{95}$ ) 10-min sections of data for bins in the middle of the water column (8–10 m above the seabed) and a range of estimates of the Reynolds stress. Samples 8 and 9 correspond to negative estimates of  $P$ .

Sample No.	$-\rho u'w'$ (Pa)	$\Delta_{95}$ (Pa)
1) High stress	0.96	$\pm 0.70$
2)	0.89	$\pm 0.70$
3)	-0.37	$\pm 0.20$
4) Lower stress	0.23	$\pm 0.20$
5)	-0.21	$\pm 0.58$
6)	0.11	$\pm 0.23$
7)	-0.07	$\pm 0.27$
8) Estimates giving $-P$	0.04	$\pm 0.57$
9)	-0.01	$\pm 0.20$

imate) is significantly different from the distribution of the random covariance estimates (i.e., lies outside the 95% significance level,  $\Delta_{95}$ ) the stress estimate can then be assumed to be reliable. Examples are given in Table A1 for a range of midwater column stress estimates oriented in the direction of the tidal flow. The high stress values (e.g., samples 1–3) all lie outside the 95% significance level. However, of the lower stress values given, only one (sample 4) is marginally significant, and the remainder of the samples are not different from zero.

The proportion of negative  $P$  estimates to the total should provide a measure of the data quality for any particular depth bin or time. For the bottom 10 depth bins the data quality is high, with negative  $P$  estimates accounting for  $< 20\%$  of the total return for each depth bin. In most cases the negative  $P$  estimates at these heights correspond to slack water. The discard rate in the depth bins near the surface was higher, reaching  $> 50\%$  for the first few hours of the deployment and around the second low water, corresponding to times when high stress values are observed (e.g., Table A2). Initially in this section we will consider the origin and consequences of the negative  $P$  estimates obtained for times of weak flow and weak stratification.

The distribution of  $\varepsilon$  measurements that coincide with the negative  $P$  estimates is given together with the distribution of the  $\varepsilon$  measurements corresponding to all the  $P$  estimates (Fig. A1). The distribution of the negative values of  $P$  is heavily biased toward low values of  $\varepsilon$ , with negative  $P$  estimates matching over one-half of the values of  $\varepsilon \leq 7 \times 10^{-5} \text{ W m}^{-3}$ . Employing the equi-

TABLE A2. Estimates of Reynolds stress in the direction of the tidal flow together with the 95% significance level ( $\Delta_{95}$ ) from 10-min sections of data for bins in the upper part of the water column during the first 2h of the observational period, which give negative estimates of  $P$ .

Sample No.	$-\rho u'w'$ (Pa)	$\Delta_{95}$ (Pa)
10) Near surface $-P$	0.15	$\pm 3.10$
11)	-0.21	$\pm 4.90$
12)	-0.36	$\pm 3.10$

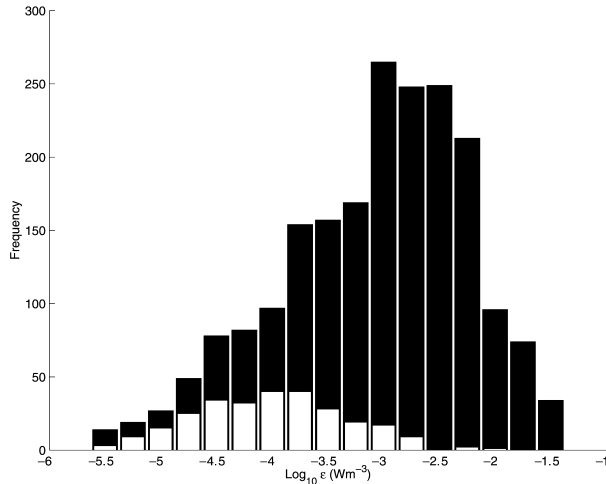


FIG. A1. The distribution of  $\varepsilon$  measurements, which correspond to estimates of  $P$  in space and time. The overlaid white histogram shows the distribution of  $\varepsilon$  measurements, which match negative  $P$  estimates in space and time.

librium assumption ( $P \approx \varepsilon$ ), this result would suggest that, below this value,  $P$  estimates are dominated by noise, and implies a lower limit for the estimation of  $P$ , using this technique and the chosen parameter settings, of  $\sim 7 \times 10^{-5} \text{ W m}^{-3}$ .

This threshold value may be compared with the theoretical estimate for the lower threshold of  $P$ . The uncertainty in the stress estimate is (Stacey et al. 1999a):

$$\sigma_R = \sqrt{\frac{3}{M} \frac{b_i'^2}{\sin^2 2\theta}}, \quad (\text{A2})$$

where  $M$  is the number of samples (300 in this case) that will have its lowest value in conditions of no flow, when  $(b_i'^2)^{1/2} = \text{instrument noise } (\sigma_N) = 0.007 \text{ m s}^{-1}$ . Combining this with the uncertainty in the shear estimate,  $\sigma_s = \sqrt{2}\sigma_H/\sqrt{M}\Delta z = 6 \times 10^{-4} \text{ s}^{-1}$ , where  $\sigma_H$  is the uncertainty in the horizontal velocity ( $\sim 0.015 \text{ m s}^{-1}$ ) data leading to a lower threshold in the estimation of  $P$  of  $5 \times 10^{-6} \text{ W m}^{-3}$ , a value that is about an order of magnitude less than that estimated above from the observations.

## APPENDIX B

### Instrument Tilt and Wave Bias in the Estimation of Stress

Modifying the along-stream part of Eq. (4) to account for instrument tilt but neglecting second and higher-order terms in the pitch and roll ( $\psi_{34}$  and  $\psi_{12}$ ) respectively gives (Lohrmann et al. 1990; Lu and Lueck 1999)

$$\overline{u'w'} = \frac{\overline{b_3'^2} - \overline{b_4'^2}}{2 \sin 2\theta} + \psi_{34}(\overline{v'^2} - \overline{w'^2}) - \psi_{12}\overline{u'v'}. \quad (\text{B1})$$

Two new terms are introduced to the rhs of the equation

associated with the tilt of the instrument. In both cases the bias introduced in the Reynolds stress estimate is proportional to the magnitude of the tilt angles. The correlation term,  $\psi_{34}\overline{u'v'}$ , will be small compared to the Reynolds stress even if  $\overline{u'v'}$  is the same order as the Reynolds stresses, provided the tilt angles are small. For example the initial roll angle,  $\psi_{12} \sim 0.5^\circ$ , will result in a bias in the along-stream stress estimate of  $< 1\%$ . The contribution of the comparable term to the bias in the small cross-stream stress term will be  $\sim 6\%$ .

The difference in variance term,  $\psi_{34}(\overline{v'^2} - \overline{w'^2})$ , will be negligible provided the turbulence is isotropic (Lohrmann et al. 1990). However, if the turbulence is anisotropic, as would be expected, for example, close to the seabed, the bias resulting from this term will be significant. Lu and Lueck (1999) estimate this term may contribute 8.5% per degree of tilt, by arguing that for anisotropic turbulence this term will be of the order  $(\psi_{34}q^2/2)$ , and assuming that the magnitude of  $q^2/2$  is approximately 5 times as large as the Reynolds stress (e.g., Gross and Nowell 1983). This result has been confirmed by observation using an acoustic Doppler velocimeter (Howarth 2003).

For the deployment reported here ( $\psi_{34,\text{max}} \sim -3.5^\circ$ ) the difference in variance term will contribute to a maximum bias of  $\sim 25\%$  in the along-stream estimate of the Reynolds stress with a maximum bias in the small cross-stream term  $\sim 3\% - 4\%$  if the turbulence is fully anisotropic. The bias in the along-stream stress due to the difference in variance term will result in an overestimate in the Reynolds stress on the flood phase of the tide of  $\sim 15\%$ , and an underestimate in the Reynolds stress on the ebb phase of the tide of  $\sim 15\%$  for a typical pitch of  $\psi_{34} \approx 2^\circ$ , but again only if the turbulence is fully anisotropic.

A possible explanation for the discrepancy between the flood and ebb ratios is the difference in variance term described above. It has been estimated that for fully anisotropic turbulence and an instrument pitch similar to that observed here, the variance method would underestimate the stress by  $\sim 15\%$  on the ebb phases of the tide and would overestimate the stress by  $\sim 15\%$  on the flood phases of the tide. However, although the pitch angle only changes slightly between the two tidal cycles, we observe a large discrepancy during the first tidal cycle but not the second. In considering the external conditions, the main difference between the two tidal cycles was the presence of a heavy swell during much of the first tidal cycle.

In order to examine the effect of surface waves on the stress estimates it is necessary to make a number of assumptions, the most fundamental of which is that wave-induced and turbulent velocity fluctuations are uncorrelated (Trowbridge 1998). One needs also to assume that the statistical properties of the waves are stationary and that the record lengths are effectively infinite (not a bad approximation because record lengths of 10 min

are taken while the observed wave period is  $\sim 5.5$  s). If the waves are assumed to be weakly nonlinear and narrow banded in both frequency and direction then three extra terms are added to the rhs of Eq. (B1) to account for the presence of waves on the stress estimate (Trowbridge 1998):

$$\begin{aligned} \overline{v'w'} = & \frac{\overline{b_3'^2} - \overline{b_4'^2}}{2 \sin 2\theta} + \psi_{34}(\overline{v'^2} - \overline{w'^2}) - \psi_{12}\overline{u'v'} \\ & - \overline{\tilde{v}\tilde{w}} + \psi_{34}(\overline{\tilde{v}^2} - \overline{\tilde{w}^2}) - \psi_{12}\overline{\tilde{u}\tilde{v}}, \end{aligned} \quad (\text{B2})$$

where the  $\tilde{u}$ ,  $\tilde{v}$ ,  $\tilde{w}$  are the contributions to the velocity from the orbital velocity of the surface waves. Order-of-magnitude estimates of the bias associated with these new terms may be estimated using the linear intermediate wave equations; for example,

$$\begin{aligned} \tilde{v} &= \frac{gak}{\sigma} \frac{\cosh k(h-z)}{\cosh kh} \sin \sigma t \\ \tilde{w} &= -\frac{gak}{\sigma} \frac{\sinh k(h-z)}{\cosh kh} \cos \sigma t, \end{aligned}$$

giving

$$\overline{\tilde{v}^2} - \overline{\tilde{w}^2} = \left(\frac{gak}{\sigma}\right)^2 \frac{1}{2 \cosh^2 kh}, \quad (\text{B3})$$

taking the observed values for wavenumber and frequency and assuming amplitude  $a = 0.5$  m gives a value (taking  $\psi_{34} = 2^\circ$ ) of  $\sim O(0.01)$  m<sup>2</sup> s<sup>-2</sup> or  $\sim O(0.5)$  Pa. The bias in the stress due to this term is sufficient to explain the ebb/flood and first tidal cycle/second tidal cycle differences in the ratio  $U_{*S}/U_{*P}$ .

Similarly,

$$\overline{\tilde{u}\tilde{v}} = \left(\frac{gak}{\sigma}\right)^2 \frac{\cosh^2 k(h-z)}{2 \cosh^2 kh} \frac{1}{2} \sin 2\chi, \quad (\text{B4})$$

where  $\chi$  is the angle of incidence of the surface waves to north. This term will lead to a maximum bias near the surface  $\sim O(-0.4)$  Pa decreasing with depth to  $\sim O(-0.04)$  Pa near the bed. In this case, the combined effect of these two terms will be to result in an overestimate in the along-stream stress estimate during the flood phase of the tide, and an underestimate during the ebb. If the surface waves are not related to the tide, these terms will produce a constant offset provided the wave field does not change.

#### REFERENCES

- Bowden, K. F., and L. A. Fairbairn, 1956: Measurements of turbulent fluctuations and Reynolds stresses in a tidal current. *Proc. Roy. Soc. London*, **A237**, 422–438.
- , —, and P. Hughes, 1959: The distribution of shearing stresses in a tidal current. *Geophys. J. Roy. Astron. Soc.*, **2** (4), 288–305.
- Dewey, R. K., and W. R. Crawford, 1988: Bottom stress estimates from vertical dissipation rate profiles on the continental shelf. *J. Phys. Oceanogr.*, **18**, 1167–1177.
- , —, A. E. Gargett, and N. S. Oakey, 1987: A microstructure instrument for profiling oceanic turbulence in coastal bottom boundary layers. *J. Atmos. Oceanic Technol.*, **4**, 288–297.
- Etamad-Shahidi, A., and J. Imberger, 2002: Anatomy of turbulence in a narrow and strongly stratified estuary. *J. Geophys. Res.*, **107**, 3070, doi:10.1029/2001JC000977.
- Gregg, M. C., 1999: Uncertainties and limitations in measuring  $\epsilon$  and  $\chi_T$ . *J. Atmos. Oceanic Technol.*, **16**, 1483–1490.
- Gross, T. F., and A. R. M. Nowell, 1983: Mean flow and turbulence scaling in a tidal boundary layer. *Cont. Shelf Res.*, **2**, 109–126.
- Howarth, M. J., 1999: Wave measurements with an ADCP. *Proc. IEEE Sixth Working Conf. on Current Measurement*, San Diego, CA, IEEE, 41–44.
- , 2003: ADCP estimation of Reynolds stress and bottom stress. *Proc. IEEE/OES Seventh Working Conf. on Current Measurement*, San Diego, CA, IEEE/OES, 219–224.
- Inall, M. E., and T. P. Rippeth, 2002: Dissipation of tidal energy and associated mixing in a wide fjord. *J. Environ. Fluid Mech.*, **2**, 219–240.
- , —, and T. J. Sherwin, 2000: The impact of non-linear waves on the dissipation of internal tidal energy at the shelf break. *J. Geophys. Res.*, **105** (C4), 8687–8705.
- Lamb, H., 1932: *Hydrodynamics*. Cambridge University Press, 738 pp.
- Lien, R.-C., and M. C. Gregg, 2001: Observations of turbulence in a tidal beam and across a coastal ridge. *J. Geophys. Res.*, **106** (C3), 4575–4592.
- Lohrmann, A., B. Hackett, and L. P. Røed, 1990: High-resolution measurements of turbulence, velocity and stress using a pulse-to-pulse coherent sonar. *J. Atmos. Oceanic Technol.*, **7**, 19–37.
- Lu, Y., and R. G. Lueck, 1999: Using a broadband ADCP in a tidal channel. Part II: Turbulence. *J. Atmos. Oceanic Technol.*, **16**, 1568–1579.
- , —, and D. Huang, 2000: Turbulence characteristics in a tidal channel. *J. Phys. Oceanogr.*, **30**, 855–867.
- Lueck, R. G., and Y. Lu, 1997: The logarithmic boundary layer in a tidal channel. *Cont. Shelf Res.*, **17**, 1785–1801.
- , and F. Wolk, 1999: An efficient method for determining the significance of covariance estimates. *J. Atmos. Oceanic Technol.*, **16**, 773–775.
- , W. R. Crawford, and T. R. Osborne, 1983: Turbulent dissipation over the continental slope off Vancouver Island. *J. Phys. Oceanogr.*, **13**, 1809–1818.
- Moum, J. N., and J. D. Nash, 2000: Topographically induced drag and mixing at a small bank on the continental shelf. *J. Phys. Oceanogr.*, **30**, 2049–2054.
- , M. C. Gregg, R. C. Lien, and M. E. Carr, 1995: Comparison of turbulence kinetic energy dissipation rate estimates from two ocean microstructure profilers. *J. Atmos. Oceanic Technol.*, **12**, 346–366.
- Nasmyth, P. W., 1970: Oceanic turbulence. Ph.D. thesis, University of British Columbia, 105 pp.
- Ninnis, R., 1984: The effects of spacial averaging on airfoil shear probe measurements of oceanic velocity microstructure. Ph.D. thesis, University of British Columbia, Vancouver, Canada, 109 pp.
- Oakey, N. S., 1982: Determination of the rate of dissipation of turbulent energy from simultaneous temperature and velocity shear microstructure measurements. *J. Phys. Oceanogr.*, **12**, 256–271.
- Osborne, T. R., and W. R. Crawford, 1980: Turbulent velocity measurements with an airfoil probe. *Instruments and Methods of Air-Sea Interaction*, L. Hasse et al., Eds., Plenum Press, 369–386.
- RDI, 1998: Workhorse ADCP. Technical Manual P/N957-6000-00, RDI, 64 pp.
- Rippeth, T. P., N. R. Fisher, and J. H. Simpson, 2001: The cycle of turbulent dissipation in the presence of tidal straining. *J. Phys. Oceanogr.*, **31**, 2458–2471.
- , E. Williams, and J. H. Simpson, 2002: Reynolds stress and

- turbulent energy production in a tidal channel. *J. Phys. Oceanogr.*, **32**, 1242–1251.
- Simpson, J. H., W. R. Crawford, T. P. Rippeth, A. R. Campbell, and J. V. S. Cheok, 1996: The vertical structure of turbulent dissipation in shelf seas. *J. Phys. Oceanogr.*, **26**, 1579–1590.
- , T. P. Rippeth, and A. R. Campbell, 2000: The phase lag of turbulent dissipation in tidal flow. *Interactions between Estuaries, Coastal Seas and Shelf Seas*, T. Yanagi Ed., TERRAPUB, Tokyo, 57–67.
- Stacey, M. T., S. G. Monismith, and J. R. Burau, 1999a: Measurements of Reynolds stress profiles in unstratified tidal flow. *J. Geophys. Res.*, **104**, 10 933–10 949.
- , —, and —, 1999b: Observations of turbulence in a partially stratified estuary. *J. Phys. Oceanogr.*, **29**, 1950–1970.
- Tropea, C., 1981: A note concerning the use of a one-component LDA to measure shear stress terms. *Exp. Fluids*, **1** (10), 209–210.
- Trowbridge, J. H., 1998: On a technique for measurement of turbulent shear stress in the presence of surface waves. *J. Atmos. Oceanic Technol.*, **15**, 290–298.

